The EMBO Journal (2008) 27, 2780–2788 | © 2008 European Molecular Biology Organization | Some Rights Reserved 0261-4189/08
www.embojournal.org

THE EMBO JOURNAL

EMBO open

Structural insights into mechanism and specificity of *O*-GlcNAc transferase

Andrew J Clarke[1], Ramon Hurtado-Guerrero[1], Shalini Pathak[1], Alexander W Schüttelkopf[1], Vladimir Borodkin, Sharon M Shepherd, Adel FM Ibrahim[2] and Daan MF van Aalten*

Division of Biological Chemistry & Drug Discovery, College of Life Sciences, University of Dundee, Dundee, UK

Post-translational modification of protein serines/threonines with *N*-acetylglucosamine (*O*-GlcNAc) is dynamic, inducible and abundant, regulating many cellular processes by interfering with protein phosphorylation. O-GlcNAcylation is regulated by *O*-GlcNAc transferase (OGT) and *O*-GlcNAcase, both encoded by single, essential, genes in metazoan genomes. It is not understood how OGT recognises its sugar nucleotide donor and performs *O*-GlcNAc transfer onto proteins/peptides, and how the enzyme recognises specific cellular protein substrates. Here, we show, by X-ray crystallography and mutagenesis, that OGT adopts the (metal-independent) GT-B fold and binds a UDP-GlcNAc analogue at the bottom of a highly conserved putative peptide-binding groove, covered by a mobile loop. Strikingly, the tetratricopeptide repeats (TPRs) tightly interact with the active site to form a continuous 120 Å putative interaction surface, whereas the previously predicted phosphatidylinositide-binding site locates to the opposite end of the catalytic domain. On the basis of the structure, we identify truncation/point mutants of the TPRs that have differential effects on activity towards proteins/peptides, giving first insights into how OGT may recognise its substrates.

The EMBO Journal (2008) **27,** 2780–2788. doi:10.1038/emboj.2008.186; Published online 25 September 2008
Subject Categories: proteins; structural biology
Keywords: glycobiology; *O*-GlcNAc; protein structure; signal transduction

Introduction

Serines/threonines on nucleoplasmic proteins in metazoans can be post-translationally modified with *N*-acetylglucosamine (*O*-GlcNAc) (Torres and Hart, 1984). This is an abundant, dynamic and inducible modification, regulating a wide range of cellular processes, such as the cell cycle, transcription, the insulin response and proteasomal degradation (Love and Hanover, 2005; Hart *et al*, 2007). There is a considerable body of evidence to suggest that *O*-GlcNAc may regulate cellular protein phosphorylation by competing for the same serines/threonines (Hart *et al*, 1995, 2007; Love and Hanover, 2005). However, in striking contrast to protein phosphorylation, dynamically regulated by over 500 kinases and 150 phosphatases, O-GlcNAcylation is balanced by a single, inverting *O*-GlcNAc transferase (OGT) and a single *O*-GlcNAc hydrolase (Haltiwanger *et al*, 1992; Gao *et al*, 2001). The genes for these proteins are highly conserved and essential in metazoans (Hanover *et al*, 2005; Hart *et al*, 2007). Despite the discovery and characterisation of OGT over two decades ago, the molecular mechanisms by which it recognises its protein substrates and transfers *O*-GlcNAc from the UDP-GlcNAc donor are not understood. Early sequence analyses suggested the presence of two conserved domains, CDI/II, separated by a linker (Lubas *et al*, 1997; Roos and Hanover, 2000), and it has also been demonstrated that OGT is a metal-independent glycosyltransferase (Kreppel *et al*, 1997; Lubas and Hanover, 2000). Unlike the protein kinases, which often possess exquisite specificity towards precise peptide sequences, no O-GlcNAcylation sequence motif has so far been discovered. In addition to recognition of protein/peptide substrates, OGT has very recently been shown to bind to phosphatidylinositides (PIs) at the plasma membrane, which is required for O-GlcNAcylation of protein kinase B, a key node in the insulin signalling pathway (Yang *et al*, 2008).

OGT possesses an unusual N terminus, consisting of 2.5–13.5 tetratricopeptide repeats (TPRs) depending on alternative splicing (Kreppel and Hart, 1999). Elegant truncation and competition experiments have demonstrated that, although not essential for short peptide substrates, these TPRs have some function in the recognition of intact protein substrates (Lubas and Hanover, 2000; Iyer and Hart, 2003). A structure of some of the N-terminal repeats revealed how these form a superhelix with a large concave surface, proposed to represent the substrate-binding groove (Jinek *et al*, 2004). However, the molecular mechanisms through which these TPRs contribute to *O*-GlcNAc transfer are not understood.

Here, using X-ray crystallography and structure-guided mutagenesis, we provide the first molecular insights into the structure of OGT, how it binds UDP-GlcNAc and aligns it for inverting *O*-GlcNAc transfer, and reveal that the TPRs are not a separate domain, but intimately associated with the active site groove, forming an extended and highly conserved putative interaction surface extending over 120 Å. We identify TPR truncations and substrate groove point mutants of OGT

*Corresponding author. Division of Biological Chemistry & Drug Discovery, College of Life Sciences, University of Dundee, Dundee DD1 5EH, UK. Tel.: +44 1382 344 979; Fax: +44 1382 385 764;
E-mail: dava@davapc1.bioch.dundee.ac.uk
[1]These authors contributed equally to this work
[2]College of Life Sciences cloning team.

Received: 15 May 2008; accepted: 21 August 2008; published online: 25 September 2008

that dissect the balance between recognition of peptides in the active site groove of about 35 Å and protein substrates by the more extended surface formed by the TPRs. The OGT structure shows that recently identified mutations that disrupt PI binding locate to a solvent-exposed pocket on the catalytic domain. This work provides a molecular framework for further studies towards OGT specificity and for the discovery/interpretation of novel OGT inhibitors.

Results and discussion

OGT adopts a GT-B fold

The CAZy database (Coutinho *et al*, 2003) shows that human OGT (hOGT) is predicted to adopt the GT41 fold, for which there are currently no known structures. To determine the OGT structure, we cloned, overexpressed and purified an apparent OGT orthologue from *Xanthomonas campestris* (*Xc*OGT). This protein is 36% identical to the hOGT sequence in the catalytic core and in addition contains three apparent TPRs (Figure 1). Native *Xc*OGT crystals diffracted to 2.1-Å resolution, and phases were obtained with a seleno-methionine (SeMet) derivative (Table I; Supplementary Figure 1). Iterative model building and refinement yielded a final model with good refinement statistics ($R = 0.194$, $R_{free} = 0.237$; Table I). Soaking experiments with a phosphonate analogue of UDP-GlcNAc yielded a complex at 2.5 Å resolution ($R = 0.217$, $R_{free} = 0.258$; Table I).

The *Xc*OGT structure reveals three distinct domains, conserved in hOGT (Figures 1 and 2). At the N terminus, three complete TPR repeats form the standard TPR superhelix (Kusuda *et al*, 1998; D'Andrea and Regan, 2003), followed by another two pairs of antiparallel α-helices, termed the TPR-like repeats (TLRs; green in Figure 2) continuing the superhelix. At the C terminus, two similar α/β-folds are observed, with the UDP-GlcNAc-binding site formed at the interface between these domains. Previous bioinformatics analysis proposed two separate catalytic/substrate-binding domains (CDI/II) (Roos and Hanover, 2000). However, structure searches with DALI (Holm and Sander, 1993) reveals that CDI/II of *Xc*OGT, and thus the GT41 family, in fact form a single catalytic domain of the GT-B fold frequently observed in GTs (Davies *et al*, 2005). Examples of inverting GT-B GTs adopting similar overall folds are MurG (Hu *et al*, 2003) (RMSD on 260 equivalent Cαs = 4.4 Å; see Supplementary Figure 2) and β-glucosyltransferase (Larivière *et al*, 2003) (RMSD on 230 equivalent Cαs = 3.3 Å). Whereas GTs adopting the GT-A fold are metal-dependent enzymes, GT-B GTs are metal-independent (Davies *et al*, 2005). There is no evidence for metal coordination in the *Xc*OGT active site, and hOGT is active in the absence of exogenous divalent cations or in the presence of excess EGTA (Figure 3A).

The high sequence identity of *Xc*OGT with the well-characterised OGTs from human (Haltiwanger *et al*, 1992), *Caenorhabditis elegans* (Hanover *et al*, 2005) and *Xenopus laevis* (Figure 1) allows us to interpret sequence conservation of these metazoan OGTs in the framework provided by the *Xc*OGT structure (Figure 2), revealing a number of striking features. Not only is the area immediately surrounding the UDP-GlcNAc-binding site conserved, but also a path of high sequence conservation is observed from the active site groove, where the *O*-GlcNAc acceptor peptides are expected to bind, all the way into the TPR repeats, which have been shown to be important for substrate specificity (Lubas and Hanover, 2000; Iyer and Hart, 2003). Although sequence identity throughout the catalytic core is high, it is apparent that the metazoan OGTs contain an extra, rather variable, loop of approximately 110 residues between the two lobes of the GT-B fold, approximately 20 Å away from the active site

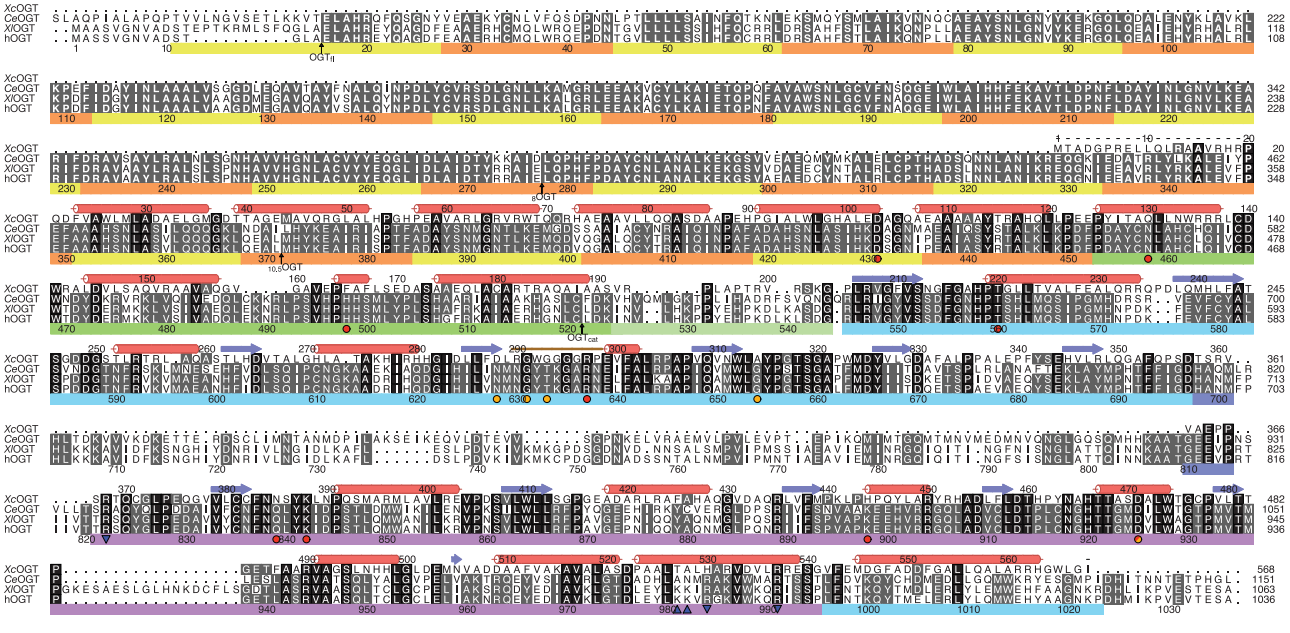

Figure 1 OGT sequence conservation. Alignment of OGT sequences from *Xanthomonas campestris* pv. *campestris* (*Xc*OGT), *Caenorhabditis elegans* (*Ce*OGT), *Xenopus laevis* (*Xl*OGT) and human (hOGT, isoform 1). N termini of hOGT constructs are indicated by arrows. Secondary structure elements (cylinders/arrows) are shown, a brown bar marks the active site lid. coloured bars indicate the TPRs (yellow = A helix; orange = B helix), the TLRs (green), the connecting loop (light green), the N-terminal GT-B subdomain (cyan), the intersubdomain linker (blue) and the C-terminal GT-B subdomain (magenta). Blue triangles give the location of the previously described (triangle up) and proposed additional (triangle down) PIP_3-interacting residues, orange and red circles locate point mutations described previously and in the present work, respectively. Labels represent hOGT/*Xc*OGT residues.

Table I Details of data collection and structure refinement

	Seleno-methionine	Apo	UDP-GlcNAc analogue complex
Unit cell (Å)	$a = 86.21$ $b = 101.44$ $c = 155.58$	$a = 81.52$ $b = 100.10$ $c = 156.27$	$a = 83.86$ $b = 100.53$ $c = 154.52$
Resolution (Å)	20.00–3.1 (3.21–3.1)	20.00–2.10 (2.17–2.10)	20.00–2.50 (2.59–2.50)
No. of observed reflections	377 707 (35 172)	300 426 (27 295)	188 629 (18 052)
No. of unique reflections	25 333 (2359)	70 020 (6362)	43 895 (4201)
Redundancy	14.9 (7.9)	4.3 (4.3)	4.3 (4.0)
$I/\sigma I$	20.8 (3.3)	14.8 (4.0)	10.2 (2.7)
Completeness (%)	99.4 (94.4)	93.5 (86.1)	95.1 (92.5)
R_{merge}	0.167 (0.651)	0.094 (0.471)	0.103 (0.389)
R, R_{free}		0.194 (0.237)	0.217 (0.258)
RMSD from ideal geometry			
Bonds (Å)		0.016	0.017
Angles (deg)		1.63	1.79
B-factor RMSD (Å^2)			
Backbone bonds		0.74	0.49
<B> (Å^2)			
Protein (no. of atoms)		39.4 (8355)	26.9 (8366)
Ligand (no. of atoms)		NA	34.8 (78)
Solvent (no. of atoms)		41.8 (321)	21.5 (148)

Values between parentheses are for the highest resolution shell. All measured data included in structure refinement. All crystals were of space group $P2_12_12_1$.
File translated from T_EX by T_TH, version 3.67 on 31 July 2008, 1833 hours.

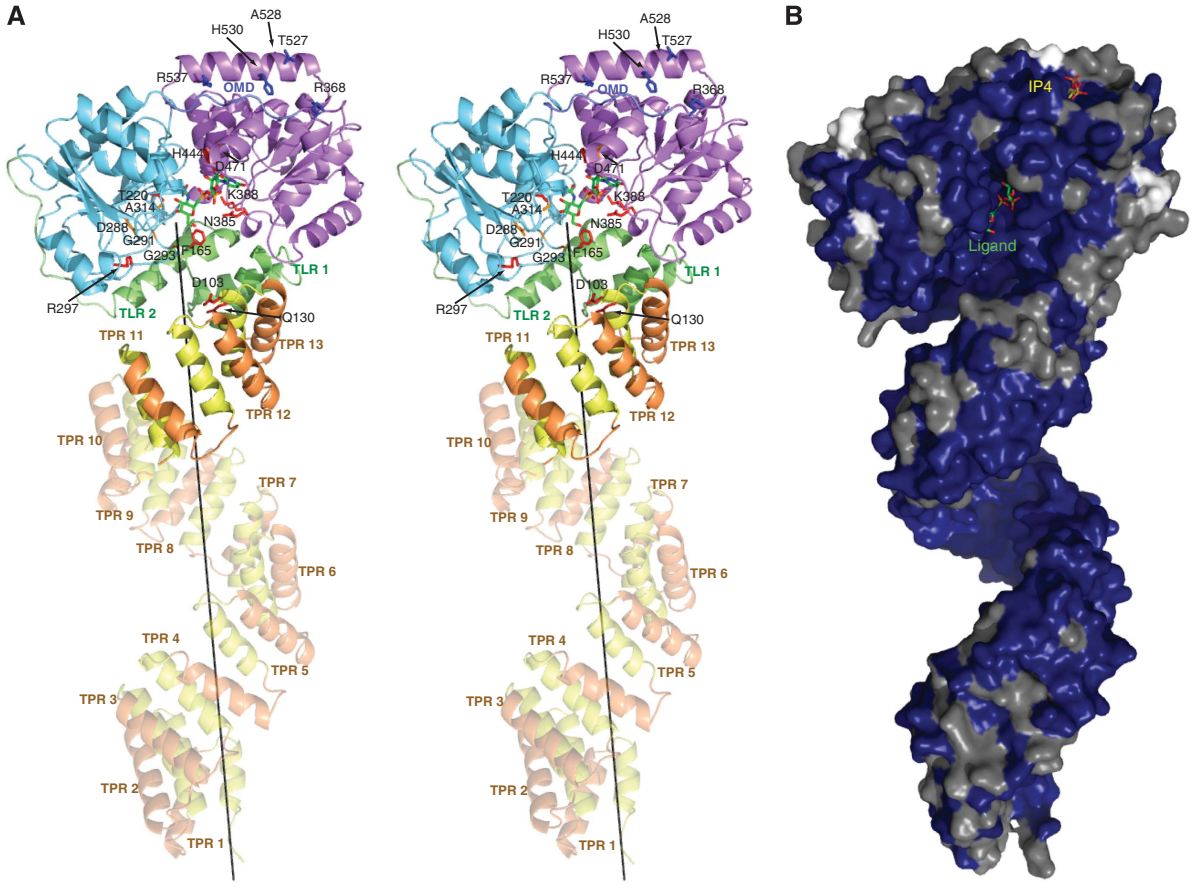

Figure 2 Structure of OGT. (**A**) Cartoon view of *Xc*OGT in complex with the UDP-GlcNAc analogue, using the domain colours as described in Figure 1. Beyond the *Xc*OGT N-terminal TPRs, the TPR superhelix is continued by the superimposed hOGT TPR structure (PDB id, 1W3B, semitransparent). The phosphoinositide-binding site is identified by an IP_4 model obtained by superposition as explained in the text. Mutated and PIP_3-binding side chains (colours as in Figure 1) are shown as sticks and labelled with *Xc*OGT residue numbers, the equivalent hOGT residue numbers can be obtained from Figure 1. The UDP-GlcNAc analogue is shown with green carbons. The OGT middle domain is indicated by the 'OMD' label. (**B**) Surface representation of the *Xc*OGT/hOGT superposition, coloured by metazoan OGT sequence conservation (blue (100% identity) to white (<50%)).

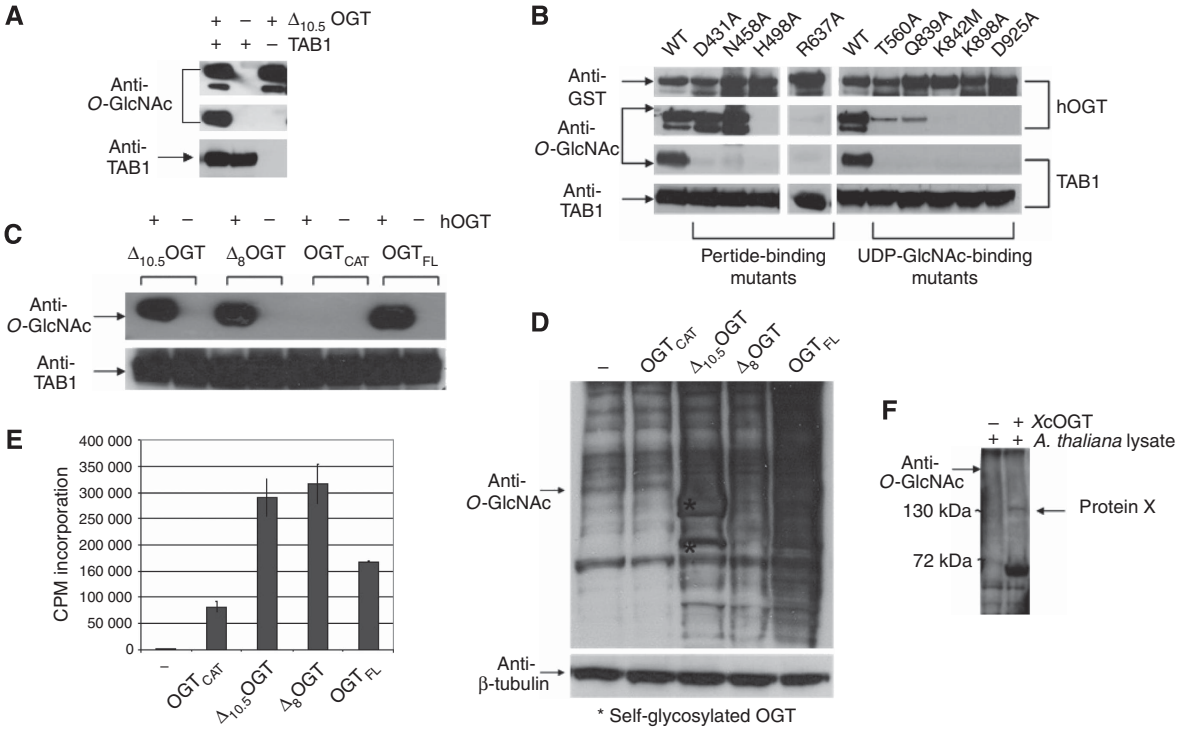

Figure 3 Mutational analysis and substrate specificity of OGT. (**A**) hOGT (overexpressed and purified from baculovirus) was incubated with the protein substrate TAB1 in the absence of magnesium and in the presence of 1 mM EGTA, and the reaction mixture was probed by anti-*O*-GlcNAc western blotting. (**B**) Single-point hOGT mutants (overexpressed and purified from *E. coli*) localised in the putative peptide and UDP-GlcNAc-binding site assayed against TAB1 and studied by anti-*O*-GlcNAc western blotting. (**C**, **D**, **E**) Activity assay of the truncated baculovirally expressed hOGT constructs against different acceptor substrates. (C) Immunoblot detecting *O*-glycosylated TAB1, (D) *O*-glycosylated HEK293 lysates and (E) radioactivity assay against the CKII peptide. (**F**) Anti-*O*-GlcNAc immunoblot of *Arabidopsis thaliana* lysate incubated with *Xc*OGT and UDP-GlcNAc shows one single protein substrate around 130 kDa.

(Figure 2) (Roos and Hanover, 2000). Secondary structure predictions suggest an α/β-fold. Although its structure/function remains to be established, it is possible that it could contribute to the relative orientations of the two lobes of the GT-B fold or perhaps acceptor substrate specificity.

A landmark study has recently revealed that hOGT translocates to the membrane and O-GlcNAcylates protein kinase B in a phosphatidylinositol(3,4,5)trisphosphate (PIP3)-dependent manner (Yang *et al*, 2008). A double mutant of two lysines, identified by lysine-scanning mutagenesis, was shown to be deficient in PIP3 binding and membrane translocation. The *Xc*OGT structure reveals that these lysines are located on the ridge of a pocket on the surface of the OGT structure (Figure 2). This pocket is well conserved in metazoan OGTs and is surrounded by further, conserved, basic residues (Arg822, Arg991 and Arg984; Figures 1 and 2). In structurally characterised phosphoinositide-binding domains, a similar arrangement is observed, with a pocket surrounded by basic residues, interacting with the phosphate groups (Lemmon, 2003). Indeed, a structural comparison of the OGT side chain positions to those of all known protein–phosphoinositide complexes produces several good matches (down to RMSD = 1.9 Å on 5 C_α positions), allowing approximate placement of a phosphoinositide in this pocket (Figure 2). This pocket is located away from the active site and TPRs; its position would thus be compatible with the PIP3-dependent O-GlcNAcylation of protein substrates such as protein kinase B (Yang *et al*, 2008) (Figure 4B).

OGT possesses a conserved UDP-GlcNAc-binding pocket

Soaking experiments of *Xc*OGT crystals with a UDP-GlcNAc phosphonate analogue revealed it to be bound in an elongated cleft (Figures 2 and 4A). UDP is tethered through backbone hydrogen bonds, a hydrogen bond to the ribose and several basic residues interacting with the phosphates. The sugar is inserted between three loops, burying the *N*-acetyl group, while leaving the β-face of the pyranose ring partially solvent exposed, compatible with the inverting nature of the enzyme (an ordered water molecule is within 3.4 Å from the anomeric carbon). One of these loops (the 'active site lid') is partially disordered and assumes different conformations in the apo/complex structures, partially (un)-covering the site of nucleophilic attack (shifts up to 11 Å; Figure 4A). Interestingly, a tyrosine hydroxyl lies near the anomeric carbon, closely interacting with a nearby lysine. It is possible that this would allow the tyrosine to function as a base, activating the peptide substrate serine/threonine hydroxyl for nucleophilic attack. His466 occupies different conformations in the apo structure and the UDP-GlcNAc phosphonate complex, interacting with the phosphates in the latter, and may participate in stabilisation of the leaving group. A number of experimental data are available to support the observed UDP-GlcNAc-binding mode and the proposed mechanism of attack. Screening of mutant collections to identify inactivating mutants of *spy*, one of the plant OGT orthologues, showed that three of these (mapping to *Xc*OGT D288, G291 and G293; Silverstone *et al*, 2007)

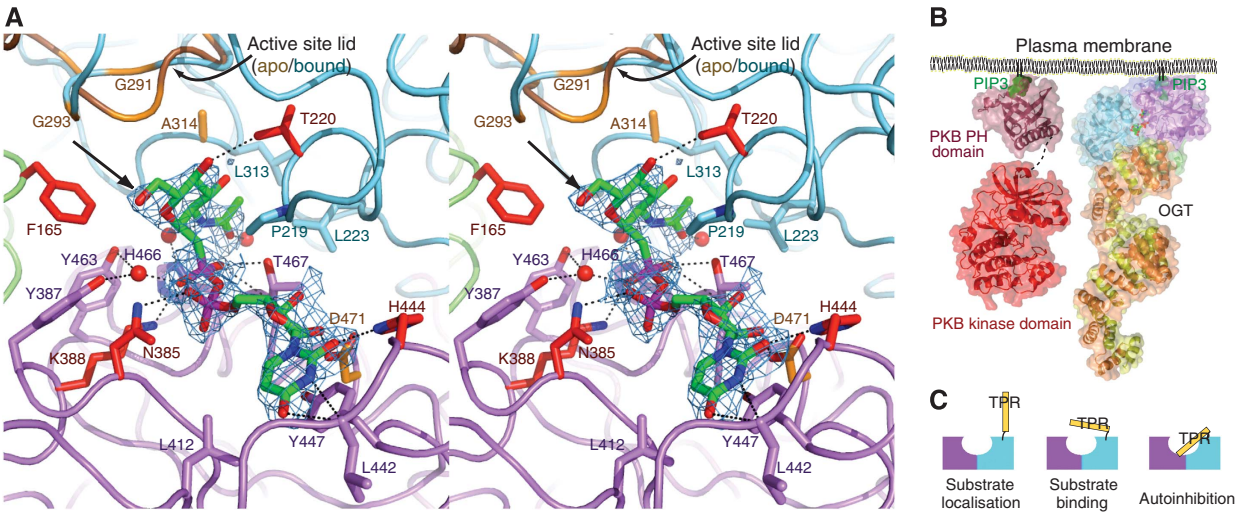

Figure 4 OGT active site and schematics of the TPR interactions. (**A**) Stereo representation of the active site of *Xc*OGT, with the UDP-GlcNAc analogue (green carbons) and an omit map (blue, 2.25σ). The protein backbone is shown as coil in domain colours as above, amino acids of interest are shown as sticks, coloured red/orange if they correspond to described point mutants in hOGT; labels as in Figure 2A. Black dotted lines indicate potential hydrogen bonds. The 'active site lid' is shown in both its apo- (brown) and ligand-bound conformation (cyan). A black arrow indicates the proposed direction of nucleophilic attack compatible with an inverting mechanism. (**B**) Model of how hOGT and protein kinase B (an OGT substrate) could colocalise in a PIP3-dependent manner on the plasma membrane, as suggested by a recent study (Yang *et al*, 2008). The OGT active site is identified by a sticks model of the sugar donor. (**C**) Cartoon representation of the OGT catalytic domain (colours as in (A, B)) and the different possible models of how the TPRs (rods) might contribute to the regulation of OGT activity, as seen in other TPR proteins, such as the widely used 'substrate localisation mode' seen in most TPR proteins (D'Andrea and Regan, 2003) and the 'autoinhibition mode' seen in protein phosphatase 5 (Yang *et al*, 2005). The crystal structure appears to be most compatible with the 'substrate-binding mode', with the TPRs tightly associated with, but not occluding, the active site.

corresponded to point mutations clustering in the mobile active site lid loop that controls access to the β-face of the sugar (Figures 2A and 4A). Furthermore, two studies have reported inactivating point mutants of hOGT, with one of these (mapping to *Xc*OGT A314) lying on the tip of a loop near the sugar (Figure 4A; Lazarus *et al*, 2005). Another reported mutant maps to *Xc*OGT D471, which hydrogen bonds the UDP ribose (Figure 4A; Yang *et al*, 2008). Most of these mutants involve residues that are conserved (Figure 1). We used additional mutagenesis in hOGT to test the UDP-GlcNAc-binding mode and the putative catalytic mechanism. Interactions with the sugar were probed through mutation T560A, which showed significantly reduced activity (Figure 3B). The K842M/Q839A point mutants were designed to disrupt interactions with the phosphates and indeed their activity is almost abrogated (Figure 3B). Similarly, the hOGT D925A/K898A mutants of residues that interact with the nucleoside show no detectable activity compared with the wild-type enzyme. An independent experiment with the hOGT D925N mutant expressed in a baculovirus system yielded similar results (see Supplementary Figure 3). Thus, the binding mode of the UDP-GlcNAc phosphonate analogue is in agreement with the mutagenesis data, although we were unable to confirm proper folding for all the inactive mutants.

The TPRs closely associate with the active site

Extensive previous work has shown that the TPRs of OGT are important for recognition of large protein substrates (Lubas and Hanover, 2000; Iyer and Hart, 2003). The structure of the N-terminal 11.5 TPRs of hOGT has been solved, revealing a superhelical structure, with asparagines on the concave surface proposed to be important for recognition of nucleoporins (Jinek *et al*, 2004). Sequence alignment of *Xc*OGT with hOGT provides a mechanism for structural alignment of the TPRs with conservation of the canonical TPR sequence motif (Figures 1 and 2). The *Xc*OGT structure reveals that the three complete *Xc*OGT repeats, corresponding to repeats 11–13 in the human sequence, closely associate with, indeed form part of, a highly conserved substrate-binding groove near the active site (Figure 2). Although soaking studies with model OGT substrate peptides were unsuccessful, the elongated nature of the groove on the catalytic domain (approximately 35 Å) suggests peptides may bind in an extended conformation.

The position of the TPRs is very different from the majority of TPR-containing proteins, where the TPRs are usually associated with the main domain through a flexible linker (D'Andrea and Regan, 2003), with the notable exception of protein phosphatase 5, where close association of the TPRs with the active site provides a mechanism for autoinhibition (Yang *et al*, 2005) (Figure 4C). Repeats 1–10 in hOGT project away from the active site. Strikingly, the central axis of the TPR superhelix points towards the sugar nucleotide in the active site (Figure 2A). This could provide a mechanism by which an elongated peptide is recognised by more than one of the TPRs while being bound in the active site groove, as has been suggested for other TPR proteins (D'Andrea and Regan, 2003). Interestingly, OGT is thought to dimerise, and residues on the convex surface of the TPRs have been shown to be involved in the dimerisation surface, and the hOGT TPR superhelix crystallised as a dimer (Jinek *et al*, 2004). However, if we use the hOGT TPR superhelix dimer as a superposition template, the resulting superposition shows the GT-B folds and the associated active sites facing away from each other, suggesting no obvious steric restrictions to the active site imposed by the TPRs in the dimer (Supplementary Figure 4).

Previous studies have shown that deletion of the first few N-terminal TPRs affects activity of OGTs towards most protein substrates, whereas deletion of 3–6 TPRs results in an enzyme that is active against short peptides only (Lubas and Hanover, 2000; Iyer and Hart, 2003). Analysis of metazoan OGT sequence conservation in the context of the available structural data provides an explanation for this. Although the active site, the putative peptide-binding groove and the last few TPR repeats possess a highly conserved surface, the concave surface of the first 3–4 TPR repeats is not well conserved (Figure 2B). This suggests that the OGTs have an evolutionarily conserved mechanism for recognising protein sequences close to the site of *O*-GlcNAc transfer, whereas different mechanisms of protein substrate recognition have a function in the terminal TPRs. To investigate this further, we designed three hOGT truncation mutants based on the structural data (Figure 1). Δ_8OGT lacks the first eight TPR repeats, whereas the remaining TPRs in the $\Delta_{10.5}$OGT truncation approximately correspond to the TPRs observed in the *Xc*OGT structure (Figures 1 and 2). Finally OGT_{cat} covers the catalytic domain only. When tested against TAB1, a key member of the TGFβ signalling pathway that we recently discovered to be an *in vitro/in vivo* OGT substrate (Pathak and van Aalten, 2008), these truncation mutants show that all but the last 2.5 TPR repeats are indispensable for recognition of TAB1 (Figure 3C). This pattern is repeated when total HEK293 cell lysate is used as acceptor substrate, showing a reduction in activity towards protein substrates when the first 8 TPRs are removed, whereas the last 2.5 TPR repeats are essential for recognition of protein substrates (Figure 3D). However, activity against a short peptide substrate is still detected even in the absence of any TPRs (Figure 3E). Furthermore, only when the first 10.5 TPR repeats are removed does OGT display significant self-glycosylation (Figure 3E). These data are in agreement with the structure, suggesting that the conserved substrate-binding groove near the sugar nucleotide is important for peptide binding, the TPRs near the active site are indispensable for activity towards all protein substrates, whereas the TPRs nearer the N terminus could contribute to recognition of specific proteins.

To further test the contribution of the last few TPRs and TLRs, we mutated residues on the conserved surfaces close to the active site and studied differences in self-glycosylation and activity towards TAB1 (Figure 3B). Strikingly, the point mutations D431A/N458A in hOGT, which line the concave surface of the TPRs/TLRs, do not inactivate the enzyme, as evidenced by abundant self-glycosylation, but no longer glycosylate the protein substrate TAB1. In contrast, the H498A/R637A mutations, located in the putative peptide-binding groove immediately adjacent to the active site, not only remove activity towards TAB1 but also abrogate self-glycosylation (Figure 3B). This is the first example of point mutations that dissect OGT's intrinsic *O*-GlcNAc transfer activity from recognition of a large protein substrate.

In most TPR-containing proteins, flexibly attached TPRs serve to associate (with) protein partners/substrates (D'Andrea and Regan, 2003) (the 'substrate localisation model'; Figure 4C). Intriguingly in protein phosphatase 5, close association of the TPR repeats with the active site provides a mechanism for autoinhibition (Yang *et al*, 2005) (the 'autoinhibition model'). It is clear that OGT represents another case, where the TPRs integrate with the active site and also serve to capture large substrates (the 'substrate-binding model'; Figure 4C). Interestingly, however, it has also been reported that a truncated form of hOGT retaining only three TPRs, exerts an effect as a dominant-negative inhibitor of other OGT isoforms, and recognises only a single protein substrate (Lazarus *et al*, 2005).

Functional characterisation of XcOGT

Although most of the substrate-binding residues are conserved between *Xc*OGT and the metazoan enzymes (Figure 1), we could not detect activity for the bacterial enzyme against bacterial and human cell lysates or short peptide substrates. To confirm that this protein would indeed be able to bind sugar nucleotides, we used surface plasmon resonance to establish a K_d of 4.2 μM for UDP-GlcNAc (data not shown), which is similar to the UDP-GlcNAc K_m values reported for hOGT (Kreppel and Hart, 1999; Lubas and Hanover, 2000). Interestingly, *X. campestris* pv. *campestris* is a phytopathogen of crucifers, such as *Arabidopsis*, invading leaf cells with the aid of virulence factors secreted through a type III secretion system. Surprisingly, we found that *Xc*OGT O-GlcNAcylates a single substrate in *Arabidopsis thaliana* cell lysates (Figure 3F), demonstrating that this is indeed an active OGT. Future identification of this substrate may give new insights into the function of bacterial OGTs. Interestingly, this restricted activity of *Xc*OGT with its limited number of TPRs has resonance with the observation that a truncated form of hOGT retaining only three TPRs recognises only a single protein substrate (Lazarus *et al*, 2005). Furthermore, the hOGT TPR truncation mutants reported here suggest an important function for the TPRs proximal to the active site in the recognition of the large protein substrate TAB1. Further studies with protein/peptide substrates in complex with OGT will be required to unravel the mechanisms of substrate recognition.

Materials and methods

Synthesis of UDP-GlcNAc phosphonate analogue

Synthesis of GlcNAc-1P phosphonate analogue was accomplished starting from the known dimethyl (2,3-*O*-isopropylidene-4,6-di-*O*-benzyl-α-D-mannopyranosyl) methanephosphonate (Borodkin *et al*, 2004) using an adaptation of published methods (Casero *et al*, 1996; Chang *et al*, 2006; Hajduch *et al*, 2008). In essence, after cleavage of the isopropylidene protection, the 3-OH group was selectively benzoylated through a dibutylstannylene intermediate. The resulting monohydroxylic compound was transformed into a 2-oxime derivative upon oxidation followed by reaction with hydroxylamine. Reduction of the oximino function with $NaBH_3CN$ in acidic methanol and hydrogenolytic reduction of the intermediate hydroxylamine in the presence of acetic anhydride afforded a separable mixture of 2-*N*-acetylamino gluco- (64%) and mannosyl methanephosphonates (12%). After swapping of all hydroxyl protective groups for acetates, the configuration of the major product was assigned as α-D-gluco using NMR spectroscopy. After removal of all but the nitrogen protecting groups (TMSBr then MeONa–MeOH), the resulting GlcNAc-1P phosphonate analogue was efficiently coupled with *N*-methylimidazolide UMP according to a recently developed procedure (Marlow and Kiessling, 2001) to furnish the targeted UDP-GlcNAc phosphonate analogue as ammonium salt in 67% yield after size-exclusion chromatography. Comparison of the 500 MHz ^1H and ^{31}P NMR spectra of the final compound with those published by others (Gordon *et al*, 2006) revealed good correlation of chemical shifts and coupling patterns.

Cloning and mutagenesis

X. campestris OGT (*Xc*OGT) coding sequence (accession: XCC0866) was amplified by PCR from genomic DNA extracted from *X. campestris* pv. *campestris* str. ATCC 33913 using the forward primer 5′-CTGGATCCATGACCGCCGACGGCCCGCGCGAGC-3′ and the reverse primer 5′-AACTCGAGCTAAATTCCCAACCAACCATGA CGCCGCGCG-3′, exploiting the *Bam*HI and *Xho*I restriction sites, for cloning into pGEX 6P-1 (GE Healthcare). hOGT (UniProtKB/Swiss-Prot O15294) is encoded by a single gene (NCBI GeneID: 8473) producing three isoforms by alternative splicing. All positional information throughout this paper refers to isoform 1 (UniProt O15294-3). The DNA sequence encoding amino-acid residues 16–1036 was obtained by PCR from IMAGE EST clone 5 017 795 using the forward primer 5′-CTGGATCCGAGTTGGCACATCGAGAATAT CAGGC-3′, and the reverse primer 5′-CTGCGGCCGCTTATGCTGACT CAGTGACTTCAACAGGC-3, and cloned, using the *Bam*HI and *Not*I restriction sites, into a version of the baculovirus protein expression vector pFastBac1 (Invitrogen), which had been modified by inserting the coding sequence for glutathione *S*-transferase (GST) followed by a PreScission protease cleavage site, resulting in the N-terminal GST fusion construct pFastBac-GST hOGT E16-end. Generation of N-terminal GST fusions of Δ_8hOGT, $\Delta_{10.5}$hOGT and $hOGT_{cat}$ (Figure 1) for expression in the baculovirus system followed the same cloning strategy following PCR amplification from the aforementioned IMAGE clone using the forward primers 5′-CTGGATCCCTACAACCACATTTCCCTGATGCTTACTG-3′ (Δ_8hOGT, starting at residue L278), 5′-CTGGATCCATGCATTATAAGGAG GCTATTCGAATCAGTCC-3′ ($\Delta_{10.5}$hOGT starting at residue M372) and 5′-CTGGATCCGTGCATCCTCATCATAGTATGCTATATCCTC-3′ ($hOGT_{cat}$ starting at residue S494), respectively, with the hOGT reverse primer shown above. The PCR products were cloned into pFastBac-GST as above.

To generate a bacterial expression construct of $\Delta_{10.5}$hOGT, an *Escherichia coli* codon-modified synthetic construct was made (Top Gene Technologies, Toronto) and cloned into the pGEX 6P-1 vector. Similar to the baculovirus $\Delta_{10.5}$ TPR hOGT expression construct, this plasmid contained the coding sequence for residues M372-A1036 of hOGT. This plasmid also served as the template for generation of amino-acid substitutions by site-directed mutagenesis. Mutated hOGT constructs with the following amino-acid substitutions were created: D431A, N458A, H498A, H558A, T560A, Y632A, R637A, R822S, Q839A, Y841F, K842M, K898A, H920A, D925A, R984S and R991S. Site-directed mutagenesis was carried out throughout following the QuikChange Site-Directed Mutagenesis protocol (Stratagene), using the KOD HotStart DNA polymerase (Novagene). All plasmids were verified by sequencing.

Expression and purification

The *Xc*OGT-pGEX-6P-1 construct was transformed into *E. coli* BL21 (DE3) pLysS cells. A Minifors fermenter (Infors) containing 3.6 l of autoinduction media + ampicillin was inoculated with 36 ml of cells. These were then grown for 48 h at 25°C, 600 r.p.m. with a constant air supply. The cells were harvested by centrifugation at 2250 *g* for 30 min, and washed in LB before being resuspended in lysis buffer (50 mM bicine pH 8.5, 150 mM NaCl, 1 mM DNAse-1, 0.1 mM lysozyme, 0.05% (v/v) β-mercaptoethanol, 0.1 mM PMSF, 1 mM benzamidine and 0.1 mM leupeptin) and lysed using a continuous flow cell disruptor (Constant Systems) at 30 kPSI. The lysate was centrifuged at 40 000 *g*, the supernatant was incubated with glutathione Sepharose 4B beads (GE Healthcare) for 2 h at 4°C on a rotating platform. The beads were then washed and incubated with PreScission Protease (200 μg protease per ml of beads) at 4°C for 16 h in buffer. The supernatant from beads and a subsequent wash were passed over a Bio-Rad 20 ml disposable column to remove the beads. This was spin concentrated to 5 ml. *Xc*OGT was further purified on a Superdex-75 26/60 column (GE Healthcare) equilibrated against 50 mM bicine pH 8.5 and 150 mM NaCl. For assay work, the protein was dialysed against 25 mM Tris pH 7.5 and 150 mM NaCl.

SeMet medium was prepared following the manufacturer's instructions (Molecular Dimensions Ltd.). The pGEX-6P-1-*Xc*OGT vector was transformed into methionine auxotrophic *E. coli* 834 (DE3). A 100 ml starter culture was grown at 37°C overnight and pelleted, washed three times with sterile H_2O, and resuspended in 1 ml water and inoculated into 1 l prewarmed (30°C) minimal media. After 30 min, 4 ml of 250 × concentrate of L-SeMet was added to the culture. Growth continued for 4 h before induction with 1 mM isopropyl β-D-1-thiogalactopyranoside (IPTG) overnight at 18°C. The protein was purified as described for native protein.

hOGT and mutants thereof were expressed in *E. coli* and baculovirus systems. For *E. coli* expression, the plasmids were transformed into BL21 (DE3) pLysS cells and plated into LB with 50 μg/ml ampicillin. Cells were grown at 37°C until $OD_{600} = 0.6$, when expression of the protein was induced with 0.2 mM IPTG at 16°C for an overnight incubation. The cells were harvested by centrifugation (3480 *g* for 30 min) and resuspended in a buffer (25 mM Tris–HCl and 250 mM sodium chloride, pH 7.5), containing lysozyme, DNAse and protease inhibitors. The cells were disrupted by the continuous flow cell disruptor at a pressure of 30 kPSI. and centrifuged at 40 000 *g* at 4°C for 30 min. The supernatant was incubated at 4°C with pre-washed glutathione Sepharose 4B beads and the proteins were eluted with 50 mM reduced glutathione in the same buffer. Subsequently, the enzymes were dialysed overnight into 25 mM Tris–HCl, 150 mM NaCl, pH 7.5 and then spin concentrated. For baculovirus expression, constructs were used to generate recombinant baculovirus using the Bac-to-Bac system (Life Technologies) following the manufacturer's protocol. The resulting baculoviruses were used to infect Sf21 cells at 1.5×10^6/ml. The infected cells were harvested by centrifugation 48 h post-infection. Cell pellets corresponding to 1–6 l of culture were resuspended in 25 mM Tris–HCl, 150 mM NaCl and 2 mM dithiothreitol (DTT) at pH 8.5, containing DNAse and protease inhibitors. The suspension was rolled at 4°C for 30 min and lysis was then performed using the continuous flow cell disruptor (35 kPSI). Centrifugation (40 000 *g*, 30 min) was then carried out. The supernatant was mixed with pre-washed glutathione Sepharose 4B beads and incubated on a rolling platform at 4°C for 1.5 h. The beads were then spun down and washed with 4 × 50 ml 25 mM Tris–HCl, 150 mM NaCl and 2 mM DTT, pH 7.8. The enzymes were then cleaved overnight at 4°C with PreScission protease and the supernatants containing the proteins were then spin concentrated. Gel filtration was carried out on a Superdex-75 XK26/60 column in 25 mM Tris–HCl, 150 mM NaCl and 2 mM DTT, pH 8.5. Fractions in the peak containing the protein were pooled and concentrated.

Structure determination

Purified *Xc*OGT protein was spin concentrated to 10 mg/ml. Hanging drop vapour diffusion crystallisation experiments were performed by mixing 1 μl of protein, 1 μl of mother liquor (0.1 M CHES pH 9.5 and 25% polyethylene glycol 3350) and 0.4 μl 100 mM praseodymium acetate. SeMet crystals were grown by mixing 1 μl of protein with 1 μl mother liquor (0.1 M CHES pH 9.0 and 27.5% PEG-3350). To obtain ligand complexes, crystals were soaked with 10 mM UDP-GlcNAc phosphonate for 5 min. Crystals were cryoprotected by a 3-s immersion in mother liquor with increased (40%) PEG-3350 concentration.

Diffraction data from *Xc*OGT, *Xc*OGT-SeMet and *Xc*OGT-UDP-GlcNAc analogue crystals were collected with synchrotron radiation and processed using the HKL suite (Otwinowski and Minor, 1997), yielding reflection files as summarised in Table I. SOLVE (Terwilliger and Berendzen, 1999) was able to locate 14 selenium sites in the SAD data set, revealing two-fold non-crystallographic symmetry, compatible with two molecules in the asymmetric unit as predicted from the Matthew's coefficient. Solvent flattening/averaging with DM (Cowtan, 1994) and RESOLVE (Terwilliger, 2003) yielded an interpretable 3.1 Å experimental map. Aided by real-space searches with known TPR structures using FFFEAR (Cowtan, 1998), a partial model was completed with COOT (Emsley and Cowtan, 2004) that was then rigid-body refined into the native data set. Iterative model building with COOT and refinement with REFMAC (Murshudov *et al*, 1997) yielded a final model covering the catalytic core and TPR repeats (Table I). This was then used as an initial model for refinement of the UDP-GlcNAc analogue complex. The UDP could be easily placed in the difference density, but two conformations appeared to be allowed for the sugar. We have refined the major conformer, placing the sugar in a conserved pocket at the bottom of the substrate-binding cleft, as assessed by omit map analysis (Figure 4A; Table I). In this complex, the active site 'lid loop' is associated with poor electron density, suggesting disorder.

OGT activity assays

The anti-*O*-GlcNAc antibody CTD110.6 was purchased from Abcam. An anti-TAB1 antibody was raised in sheep against bacterially expressed His-TAB1. A GST–HRP antibody was purchased from

Bethyl Laboratories. β-Tubulin antibody was purchased from Cell Signaling Technology. Secondary antibodies conjugated to horseradish peroxidase were from Pierce.

For western blotting, cells were lysed in lysis buffer containing 50 mM Tris–HCl pH 7.5, 150 mM NaCl, 0.5% NP40. Protein concentration was determined by Coomassie protein assay (Pierce). For immunoblotting, the protein samples were subjected to 10% SDS–PAGE, transferred to PVDF membrane and blocked with 3% BSA before incubating with primary antibody and subsequently with conjugated anti-mouse IgM-HRP. To detect proteins, a chemiluminescent signal was developed using a GE Healthcare ECL kit.

Mammalian cell lysate was prepared from HEK293 cells. Cells were harvested by the removal of the medium followed by lysis in ice cold buffer A (50 mM Tris–HCl pH 7.5, 0.1 mM EGTA, 1 mM EDTA, 1% (w/w) Triton X-100, 1 mM Na_3VO_4, 50 mM NaF, 5 mM sodium pyrophosphate, 0.27 M sucrose, 0.1% (v/v) 2-mercaptoethanol and proteinase inhibitor cocktail). Protein concentrations of the lysates were determined using the Bradford method. Recombinant TAB1 was produced in *E. coli* as a GST fusion protein.

OGT peptide assays were performed as described earlier (Iyer and Hart, 2003). The peptide PGGSTPVSSANMM (CKII peptide) was used for radioactivity assays. The peptide (1 mM) was incubated with 2 μM of the different TPR deletion mutants in the reaction buffer containing 50 mM Tris–HCl, pH 7.5, 1 mM DTT, 12.5 mM $MgCl_2$, 1 μCi of UDP-(^{3}H)GlcNAc (American Radiolabeled Chemicals) for 90 min at 37°C. After the reaction, the peptides were cleaned on a Sep-pak C18 cartridge (Waters Corp.) as follows: after washing the cartridge with 10 ml of methanol, 10 ml of 50 mM formic acid, the reaction was then loaded, followed by washing with 10 ml of 50 mM formic acid, 10 ml of 50 mM formic acid containing 0.5 M NaCl and 10 ml of distilled H_2O. The peptides were eluted from the cartridge directly into scintillation vials with 2 × 1.5 ml of methanol. After drying off the methanol, the peptides were resuspended in the scintillation fluid and taken for counting.

The *in vitro* activity assays of wild-type and mutant hOGT with 10 μM recombinant TAB1 were carried out using the same reaction conditions as for the peptide assay, in 20 μl assay volumes. The reactions were incubated for 90 min at 37°C, stopped by adding 4 × SDS–PAGE sample buffer, resolved on SDS–PAGE and after transfer were taken for probing with antibodies.

The activity of the hOGT TPR truncation mutants was also tested on the total cell lysate from HEK293 cells. The cell lysates (25 μg) were incubated with the enzymes in the standard reaction conditions, subjected to SDS–PAGE followed by western blotting. The loading controls were measured using β-tubulin antibodies after stripping the blots following detection of *O*-GlcNAc signals.

For the *Xc*OGT assays, *A. thaliana* lysate was prepared from cell suspension culture in the buffer described earlier. After addition, the buffer cells were sonicated for 30 s and centrifuged at 14 000 r.p.m. for 10 min and the supernatant was collected. For the activity assay, the lysate was heat treated for 30 min at 60°C before incubating 25 μg of the lysate in a 20 μl reaction buffer with 4 mM UDP-GlcNAc and 5 μM of *Xc*OGT. After 3 h at 37°C, the reaction was stopped by adding SDS loading buffer and taken for immunoblotting.

Supplementary data

Supplementary data are available at *The EMBO Journal* Online (http://www.embojournal.org).

Acknowledgements

We thank the Diamond Light Source/European Synchrotron Radiation Facility for beam time. This study was supported by a Wellcome Trust Senior Research Fellowship and the Lister Institute for Preventive Medicine Research Prize. We thank David Blair and Mark Agacan for experimental assistance. The coordinates and structure factors have been deposited with the PDB (entry 2VSY).

References

Borodkin VS, Ferguson MAJ, Nikolaev AV (2004) Synthesis of potential bisubstrate inhibitors of *Leishmania* elongating α-D-mannosyl phosphate transferase. *Tetrahedron Lett* **45:** 857–862

Casero F, Cipolla L, Lay L, Nicotra F, Panza L, Russo G (1996) Stereoselective Synthesis of the Isosteric Phosphono Analogues of N-Acetyl-alpha-D-glucosamine 1-Phosphate and N-Acetyl-alpha-D-mannosamine 1-Phosphate. *J Org Chem* **61:** 3428–3432

Chang R, Vo T, Finney N (2006) Synthesis of the C1-phosphonate analog of UDP-GlcNAc. *Carbohydr Res* **341:** 1998–2004

Coutinho PM, Deleury E, Davies GJ, Henrissat B (2003) An evolving hierarchical family classification for glycosyltransferases. *J Mol Biol* **328:** 307–317

Cowtan K (1994) *Joint CCP4 and ESF-EACBM Newsletter on Protein Crystallography* **31:** 34–38

Cowtan K (1998) Modified phased translation functions and their application to molecular fragment location. *Acta Crystallogr D Biol Crystallogr* **54:** 750–756

D'Andrea L, Regan L (2003) TPR proteins: the versatile helix. *Trends Biochem Sci* **28:** 655–662

Davies GJ, Gloster TM, Henrissat B (2005) Recent structural insights into the expanding world of carbohydrate-active enzymes. *Curr Opin Struct Biol* **15:** 637–645

Emsley P, Cowtan K (2004) Coot: model-building tools for molecular graphics. *Acta Crystallogr D Biol Crystallogr* **60:** 2126–2132

Gao Y, Wells L, Comer FI, Parker GJ, Hart GW (2001) Dynamic O-glycosylation of nuclear and cytosolic proteins––cloning and characterization of a neutral, cytosolic beta-*N*-acetylglucosaminidase from human brain. *J Biol Chem* **276:** 9838–9845

Gordon R, Sivarajah P, Satkunarajah M, Ma D, Tarling C, Vizitiu D, Withers S, Rini J (2006) X-ray crystal structures of rabbit *N*-acetylglucosaminyltransferase I (GnT I) in complex with donor substrate analogues. *J Mol Biol* **360:** 67–79

Hajduch J, Nam G, Kim E, Fraehlich R, Hanover J, Kirk K (2008) A convenient synthesis of the C-1-phosphonate analogue of UDP-GlcNAc and its evaluation as an inhibitor of O-linked GlcNAc transferase (OGT). *Carbohydr Res* **343:** 189–195

Haltiwanger R, Blomberg M, Hart G (1992) Glycosylation of nuclear and cytoplasmic proteins. Purification and characterization of a uridine diphospho-*N*-acetylglucosamine:polypeptide beta-*N*-acetylglucosaminyltransferase. *J Biol Chem* **267:** 9005–9013

Hanover JA, Forsythe ME, Hennessey PT, Brodigan TM, Love DC, Ashwell G, Krause M (2005) A *Caenorhabditis elegans* model of insulin resistance: altered macronutrient storage and dauer formation in an OGT-1 knockout. *Proc Natl Acad Sci USA* **102:** 11266–11271

Hart G, Greis K, Dong L, Blomberg M, Chou T, Jiang M, Roquemore E, Snow D, Kreppel L, Cole R (1995) O-Linked *N*-acetylglucosamine: the 'yin-yang' of Ser/Thr phosphorylation? Nuclear and cytoplasmic glycosylation. *Adv Exp Med Biol* **376:** 115–123

Hart GW, Housley MP, Slawson C (2007) Cycling of O-linked beta-*N*-acetylglucosamine on nucleocytoplasmic proteins. *Nature* **446:** 1017–1022

Holm L, Sander C (1993) Protein structure comparison by alignment of distance matrices. *J Mol Biol* **233:** 123–138

Hu Y, Chen L, Ha S, Gross B, Falcone B, Walker D, Mokhtarzadeh M, Walker S (2003) Crystal structure of the MurG:UDP-GlcNAc complex reveals common structural principles of a superfamily of glycosyltransferases. *Proc Natl Acad Sci USA* **100:** 845–849

Iyer S, Hart G (2003) Roles of the tetratricopeptide repeat domain in *O*-GlcNAc transferase targeting and protein substrate specificity. *J Biol Chem* **278:** 24608–24616

Jinek M, Rehwinkel J, Lazarus BD, Izaurralde E, Hanover JA, Conti E (2004) The superhelical TPR-repeat domain of O-linked GlcNAc transferase exhibits structural similarities to importin alpha. *Nat Struct Mol Biol* **11:** 1001–1007

Kreppel L, Blomberg M, Hart G (1997) Dynamic glycosylation of nuclear and cytosolic proteins. Cloning and characterization of a unique *O*-GlcNAc transferase with multiple tetratricopeptide repeats. *J Biol Chem* **272:** 9308–9315

Kreppel L, Hart G (1999) Regulation of a cytosolic and nuclear *O*-GlcNAc transferase. Role of the tetratricopeptide repeats. *J Biol Chem* **274:** 32015–32022

Kusuda K, Kobayashi T, Ikeda S, Ohnishi M, Chida N, Yanagawa Y, Shineha R, Nishihira T, Satomi S, Hiraga A, Tamura S (1998) Mutational analysis of the domain structure of mouse protein phosphatase 2Cbeta. *Biochem J* **332** (Part 1)**:** 243–250

Larivière L, Gueguen-Chaignon V, Moréra S (2003) Crystal structures of the T4 phage beta-glucosyltransferase and the D100A mutant in complex with UDP-glucose: glucose binding and identification of the catalytic base for a direct displacement mechanism. *J Mol Biol* **330:** 1077–1086

Lazarus BD, Roos MD, Hanover JA (2005) Mutational analysis of the catalytic domain of O-linked *N*-acetylglucosaminyl transferase. *J Biol Chem* **280:** 35537–35544

Lemmon M (2003) Phosphoinositide recognition domains. *Traffic* **4:** 201–213

Love DC, Hanover JA (2005) The hexosamine signaling pathway: deciphering the '*O*-GlcNAc code'. *Sci STKE* **312:** 1–14

Lubas W, Frank D, Krause M, Hanover J (1997) O-Linked GlcNAc transferase is a conserved nucleocytoplasmic protein containing tetratricopeptide repeats. *J Biol Chem* **272:** 9316–9324

Lubas WA, Hanover JA (2000) Functional expression of O-linked GlcNAc transferase––domain structure and substrate specificity. *J Biol Chem* **275:** 10983–10988

Marlow A, Kiessling L (2001) Improved chemical synthesis of UDP-galactofuranose. *Org Lett* **3:** 2517–2519

Murshudov GN, Vagin AA, Dodson EJ (1997) Refinement of macromolecular structures by the maximum-likelihood method. *Acta Crystallogr D Biol Crystallogr* **53:** 240–255

Otwinowski Z, Minor W (1997) Processing of X-ray diffraction data collected in oscillation mode. *Methods Enzymol* **276:** 307–326

Pathak S, van Aalten DMF (2008) Effects of TAK1 kinase binding protein 1 O-GlcNAcylation and its effects on the TAK1 pathway. (manuscript in preparation)

Roos M, Hanover J (2000) Structure of O-linked GlcNAc transferase: mediator of glycan-dependent signaling. *Biochem Biophys Res Commun* **271:** 275–280

Silverstone A, Tseng T, Swain S, Dill A, Jeong S, Olszewski N, Sun T (2007) Functional analysis of SPINDLY in gibberellin signaling in *Arabidopsis*. *Plant Physiol* **143:** 987–1000

Terwilliger TC (2003) SOLVE and RESOLVE: automated structure solution and density modification. *Methods Enzymol* **374:** 22–37

Terwilliger TC, Berendzen J (1999) Automated MAD and MIR structure solution. *Acta Crystallogr D Biol Crystallogr* **55:** 849–861

Torres CR, Hart GW (1984) Topography and polypeptide distribution of terminal *N*-acetylglucosamine residues on the surfaces of intact lymphocytes––evidence for O-linked GlcNAc. *J Biol Chem* **259:** 3308–3317

Yang J, Roe S, Cliff M, Williams M, Ladbury J, Cohen P, Barford D (2005) Molecular basis for TPR domain-mediated regulation of protein phosphatase 5. *EMBO J* **24:** 1–10

Yang X, Ongusaha P, Miles P, Havstad J, Zhang F, So W, Kudlow J, Michell R, Olefsky J, Field S, Evans R (2008) Phosphoinositide signalling links *O*-GlcNAc transferase to insulin resistance. *Nature* **451:** 964–969

